

# Experimental Studies With a 9F Forward-Looking Intracardiac Imaging and Ablation Catheter

Douglas N. Stephens, MS, Matthew O'Donnell, PhD, Kai Thomenius, PhD, Aaron Dentinger, PhD, Douglas Wildes, PhD, Peter Chen, PhD, K. Kirk Shung, PhD, Jonathan Cannata, PhD, Pierre Khuri-Yakub, PhD, Omer Oralkan, PhD, Aman Mahajan, MD, PhD, Kalyanam Shivkumar, MD, PhD, David J. Sahn, MD

## Abbreviations

cMUT, capacitive micromachined ultrasound transducer; EP, electrophysiology; FBW, fractional bandwidth; ML, microlinear; PZT, lead zirconate titanate; RF, radio frequency; RFA, radio frequency ablation; 3D, 3-dimensional; 2D, 2-dimensional

Received September 15, 2008, from the University of California, Davis, California USA (D.N.S.); University of Washington, Seattle, Washington USA (M.O.); GE Global Research, Schenectady, New York USA (K.T., A.D., D.W.); Irvine Biomedical Inc/St Jude Medical, Irvine, California USA (P.C.); University of Southern California, Los Angeles, California USA (K.K.S., J.C.); Stanford University, Palo Alto, California USA (P.K.-Y., O.O.); University of California, Los Angeles, California USA (A.M., K.S.); and Oregon Health & Science University, Portland, Oregon USA (D.J.S.). Revision requested October 12, 2008. Revised manuscript accepted for publication October 31, 2008.

For the assembly and testing of prototypes, we thank Ruibin Liu and Jay Williams of the University of Southern California and Rick Kust and Hien Nguyen of Irvine Biomedical, Inc. Essential animal laboratory aid and experimental data management were provided by Gina Akopyan of the University of California, Los Angeles, and by Simon Pranaitis of St Jude Medical. This research was supported by National Heart, Lung, and Blood Institute Bioengineering Research Partnership grant R01 HL67647, "High-Frequency Ultrasound Arrays for Cardiac Imaging." Drs Thomenius, Dentinger, and Wildes work for GE Global Research, and Dr Chen was president of Irvine Biomedical Inc at the time this article was written; they are also among the partners to the grant. None of the other authors has any conflict of interest with the material in this article.

Address correspondence to David J. Sahn, MD, Department of Pediatric Cardiology, Oregon Health & Science University, 3181 SW Sam Jackson Park Rd, L608, Portland, OR 97239-3098 USA.  
E-mail: sahdnd@ohsu.edu

**Objective.** The purpose of this study was to develop a high-resolution, near-field-optimized 14-MHz, 24-element broad-bandwidth forward-looking array for integration on a steerable 9F electrophysiology (EP) catheter. **Methods.** Several generations of prototype imaging catheters with bidirectional steering, termed microlinear (ML), were built and tested as integrated catheter designs with EP sensing electrodes near the tip. The wide-bandwidth ultrasound array was mounted on the very tip, equipped with an aperture of only 1.2 by 1.58 mm. The array pulse echo performance was fully simulated, and its construction offered shielding from ablation noise. Both ex vivo and in vivo imaging with a porcine animal model were performed. **Results.** The array pulse echo performance was concordant with Krimholtz-Leedom-Matthaei model simulation. Three generations of prototype devices were tested in the right atrium and ventricle in 4 acute pig studies for the following characteristics: (1) image quality, (2) anatomic identification, (3) visualization of other catheter devices, and (4) for a mechanism for stabilization when imaging ablation. The ML catheter is capable of both low-artifact ablation imaging on a standard clinical imaging system and high-frame rate myocardial wall strain rate imaging for detecting changes in cardiac mechanics associated with ablation. **Conclusions.** The imaging resolution performance of this very small array device, together with its penetration beyond 2 cm, is excellent considering its very small array aperture. The forward-looking intracardiac catheter has been adapted to work easily on an existing commercial imaging platform with very minor software modifications. **Key words:** ablation; electrophysiology; interventional guidance; intracardiac ultrasound array; miniaturized.

**I**nterventional procedures have shown continued popularity as a means to treat serious dysrhythmias such as atrial fibrillation, for which the lifetime risk has been estimated at 1 per 4 for men and women older than 40 years.<sup>1</sup> Because interventional ablation procedures to correct cardiac arrhythmias have doubled every year between 1995 and 2002,<sup>2</sup> a projection from this dramatic growth rate suggests a current annual procedure count of more than 1 million worldwide.

The catheter-based ablation procedure has revolutionized the management of cardiac arrhythmias.<sup>3-6</sup> It has transformed the field of cardiac electrophysiology (EP) from a diagnostic tool to a potent treatment method. Catheter ablation is now performed for virtually every type of arrhythmia, including Wolff-Parkinson-White syndrome,<sup>3,4</sup> concealed accessory pathways,<sup>3,4</sup> atrioventricular nodal reentrant tachycardia,<sup>7</sup> atrial flutter,<sup>8</sup> atrial fibrillation,<sup>9</sup> incisional atrial reentrant tachycardia,<sup>10</sup> and ventricular tachycardia.<sup>7</sup> Catheter ablation is also performed in all chambers of the heart and in patients with diverse structural cardiac abnormalities.<sup>11</sup>

As currently practiced, multiple electrode-tipped catheters are placed in the heart, and intracardiac electrographic signals derived from these electrodes are displayed on a computer interface monitor. Pacing and pharmacologic maneuvers are then performed to understand the cardiac electrical system and the cause of the arrhythmia. Once the arrhythmia substrate has been elucidated, catheter ablation is attempted to destroy the substrate. A common energy source for ablation is radio frequency (RF) current. A special catheter, equipped with 1 or more RF electrodes and a temperature sensor at the tip, is placed in the area of interest and connected to an RF generator producing a signal at about 500 kHz.<sup>11</sup> This energy applied to tip electrodes in contact with cardiac tissue can create heating of the distal electrode tip from 50° to 70°C, which is transmitted to the adjacent cardiac tissue, resulting in irreversible cell death and heat necrosis of the underlying tissue.<sup>12</sup> Blood can electrically conduct the radio frequency ablation (RFA) energy, but a good electromechanical contact between the catheter electrode tip and the heart surface itself is an essential prerequisite for sufficient energy concentration and successful ablation. The diameter and depth of a focal lesion can be small (about 3 mm when a 7F 4-mm tipped catheter is used), which allows precision but requires pinpoint accuracy for the best results. If highly accurate spatial localization can be determined, the ablation can be optimized to avoid the destruction of adjacent normal tissue.

Currently, there are 3 approaches to spatial navigation and anatomic localization. They are fluoroscopy, echocardiography, and electroanatomic mapping.

Fluoroscopy is the most established technique for navigating any body system, including the heart. With fluoroscopy and electrode catheters, a combined electroanatomic picture of the heart is formed, which then serves as the template for targeting the appropriate area for ablation. However, fluoroscopy has a number of disadvantages for anatomic localization. Much of the localization derived by fluoroscopy involves the experience of the operator to intelligently project the site of a catheter based on the fluoroscopic picture combined with the electrogram derived from the catheter, forming a cogent view of the anatomy. Second, it is not possible to see the finer detail of the intracardiac anatomy with fluoroscopy, even with adjunctive techniques such as radiopaque dye injections. Third, fluoroscopy cannot define the adequacy of contact of the ablating catheter to the cardiac surface, a factor that is vitally important in determining the success of ablation. Last, fluoroscopy exposes the patient to ionizing radiation, and the long-term side effects of this approach are unclear, particularly in children.<sup>13</sup> For these reasons, fluoroscopy as currently used is not the best answer to the issue of anatomic localization for catheter ablation procedures.

Echocardiography, as an extracardial imaging perspective, has not proved to be a very useful technique for catheter ablation procedures. It is sometimes used as an adjunctive method to provide additional localization to understand specific anatomic issues in particular patients. It can be performed via the transthoracic or transesophageal route. Transthoracic echocardiography suffers from the problem of poor anatomic windows, particularly in adults. Transesophageal echocardiography can now provide advanced features such as 4-dimensional imaging, and it offers a better window for the ultrasound beam to reach the heart but requires sedation or anesthesia. Both techniques can provide better detail of specific portions of the heart but are limited by their 2-dimensional (2D) displays. Although echocardiography has been described as an adjunct to fluoroscopy, it has not displaced the need for fluoroscopy in catheter ablation procedures.

In the last few years, a commercial device, the AcuNav (Siemens Medical Solutions, Malvern,

PA), has been widely used in EP procedures<sup>14-16</sup>; it is a side-looking 5.5- to 10-MHz, 64-element linear phased array capable of providing multi-modal ultrasound imaging in both 8F and 10F sizes. The AcuNav device was recently licensed to Biosense Webster, Inc (Diamond Bar, CA), and its next-generation device, the SoundStar, is now interfaced with Biosense Webster guidance systems: the Carto XP EP navigation system, the Carto RMT electroanatomic mapping system, and the CartoMerge image integration software. There has been considerable interest in this device, especially for its potential to replace transesophageal echocardiography in interventional procedures. To date, however, there have been mixed reports of success with this particular method of electroanatomic mapping.<sup>17-20</sup>

Another intracardiac device, the ViewFlex catheter, manufactured by EP Med Systems (St Jude Medical, St Paul, MN), is a single-use 9F catheter operating at up to 14 MHz and is bidirectionally steerable. The introduction of the ViewMate 2 ultrasound platform, which had been developed in conjunction with Philips Healthcare (Bothell, WA), provides improved quality ultrasound, color flow, and tissue Doppler imaging.

Electroanatomic mapping is a newer technique for anatomic localization within the heart; it has been developed over the last decade in several different formats.<sup>8,21-23</sup> Procedurally, by first using fluoroscopy and electrographic data, a virtual heart model can be derived.<sup>24-26</sup> After this has been done, the catheter position within the heart model can be continuously tracked by an electromagnetic sensing method, which can produce volumetric mapping, thereby eliminating the need for fluoroscopy. The most important advantage of this technique is the elimination of fluoroscopy. Unfortunately, it cannot directly help in understanding the finer detail of cardiac anatomy.

We have reported on the development of a side-looking EP-enabled intracardiac imaging catheter called the hockey stick,<sup>27,28</sup> which provides high-resolution imaging, tissue Doppler imaging for studies of rhythm propagation, EP recording, and integration with the NavX (EnSite NavX navigation and visualization technology; St Jude Medical) 3-dimensional (3D) electroanatomic navigation method.

Novel and compelling efforts in a forward-looking catheter imaging perspective have been made previously<sup>29-34</sup> but have had limitations in size, steering, or compatibility with a standard imaging system platform. In this article, we report the development of a forward-looking intracardiac ultrasound catheter designed for both ablation guidance with high-frequency near-field imaging resolution and operation on a standard commercial imaging system.

## Materials and Methods

### *An EP Forward-Looking Catheter With a 14-MHz Piezoelectric Microlinear Array*

The microlinear (ML) catheter construction with dimensions of 9F in diameter and 110 cm in length is based on a standard EP catheter shaft design with metal braid reinforcement and catheter tip steering control enabled through the use of 2 steering wires, each with its own very small wall lumen on opposite sides of the catheter shaft. The 24-element array microcoax cables (48 American wire gauge, each at 0.0065 inch in diameter; Precision Interconnect, Portland, OR) and EP electrode sensor internal wires (insulated and each at 0.006 inch) are contained easily in the central lumen of the 9F ML catheter shaft. As used with the hockey stick catheter,<sup>28</sup> the ML catheter electrical connections were made with a custom interface. The imaging coaxial cables are terminated in a special adapter that connects to a custom interface box, which is in turn connected to an imaging system zero insertion force connector with a 2-m nondisposable cable assembly. The EP wire connections are separately handled because they are terminated in a standard connector suitable for a direct interface to standard EP monitoring equipment.

The forward-looking ML catheter distal tip itself, however, is quite different from the distal tip of the side-looking hockey stick catheter. Because the array design is rectangular and flat-end facing, the 25- $\mu$ m-thick, 2-sided flex circuit on which the array is mounted must be folded in 2 places at 90° with bend radii each of approximately 0.25 mm (to fit within the distal tip housing Figure 1). We explored the use of two very different types of arrays for the ML catheter;

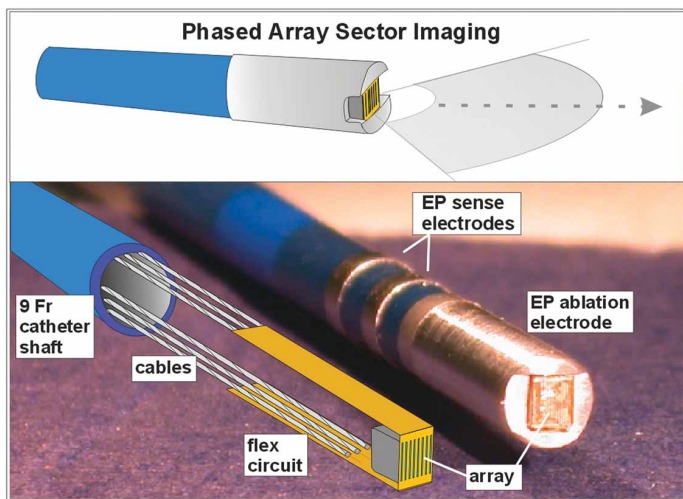


**Figure 1.** The 14-MHz, 24-element phased array forward-looking ML catheter tip region is shown. A completely equipped mechanical prototype is shown with its internal structures, including the PZT array, flex circuit, and cabling (bottom left).

one array design is piezoceramic based with the flex circuit mounted on the front side of the array, and the other design is a microelectromechanical system silicon-based capacitive micromachined ultrasound transducer (cMUT),<sup>34</sup> which is arranged with the flex circuit on the back side of the cMUT array. Both of these array types were assembled with the same element dimensions, as shown in Table 1. The work presented here, however, was limited for brevity to the construction, bench performance, and animal testing of the imaging capabilities of the piezoceramic array device only.

The ML array construction is simple because of its very small size. With regard to the piezoceramic array, the flex circuit itself and a single thin

polylene layer serve as the effective acoustic matching layers. The piezoceramic array is designed as a 2-2 composite structure using a high-dielectric ceramic (L155N; TFT Corp, Tokyo, Japan), which has proved more reliable during fine dicing than the TRS-HK1 ceramic (TRS Technologies, Inc, State College, PA), which had been used previously in the larger-pitch hockey stick array. The core ML array design is based on a stacked structure in which one piezoceramic “layer” in the 2-2 lead zirconate titanate (PZT) composite defines a single element before bonding the array to the flex circuit. The composite is 112 μm thick with 50-μm-wide piezoceramic “stacked” elements and 15-μm epoxy-filled kerfs. The front-side materials are a 25-μm-thick polyimide flex circuit with 4.5-μm metal traces that make an electrical contact by compression through the bonding epoxy with the 2-2 composite structure and a parylene layer at 10 μm of thickness to serve as an insulating outer layer that prevents the flex circuit outside (ground shield) metal from touching biological tissue. The backing is a cast-on electrically conductive reference electrode side (E-Solder 3022; Von Roll Isola USA, Inc, New Haven, CT) of approximately 1 mm in thickness. The ML array flex circuit assembly places the active signal wiring on the inside flex bend where solder connections to the internal coaxial cabling are made along with the ground wire connecting the piezoceramic grounded back-side connection in a similar way as the hockey stick array. This straightforward connection scheme allows for direct integration with the Vivid 7 Dimension imaging system (GE Vingmed Ultrasound AS, Horten, Norway).

**Table 1.** Lead Zirconate Titanate and cMUT Acoustic Array Design Parameters

| Design Parameter                                 | Acoustic Array Design Type |                                  |
|--|----------------------------|----------------------------------|
|  | Piezoceramic               | MEMS Silicon                     |
| Transducer type                                  | 2-2 composite PZT          | cMUT disk or rectangle prototype |
| Generation                                       | 1      2                   |                                  |
| Catheter size, F                                 | 15/10.2                    | 9                                |
| Transducer placement on flex circuit bend radius | Inside      Inside         | In catheter assembly<br>Outside  |
| Array elements                                   | 24      24                 | 24                               |
| Center frequency, MHz                            | 14      14                 | 14                               |
| Array pitch, mm                                  | 0.065      0.065           | 0.065                            |
| Element elevation, mm                            | 1.2      1.2               | 1.2                              |

MEMS indicates microelectromechanical system.

The ML array is optimized for noisy catheter laboratory environments by using a thin (3- $\mu\text{m}$ ) crosshatch matrix metal ground shield on the entire outside bend surface of the flex circuit. Through-hole vias are used in the flex circuit to join the outer metal shield to the inside flex circuit surface coaxial bond pad region.

The first-generation ML arrays were fabricated with 9F catheter shafts and large 15F (5-mm) tip enclosures. This was done to avoid trace breaking and stress damage of the piezoceramic array after bending of the flex circuit following early assembly attempts. Improved assembly handling techniques resulted in a reduction in the flex bend radius, which allowed smaller core assemblies. The original ML flex circuit was quite short at 13.6 mm; the second-generation design was extended to 120 mm to augment the ML catheter tip flexibility by eliminating the relatively stiff set of 24 microcoax cables in the distal tip region. The new longer flex circuit construction includes solder mask protection of the electrical traces in the long flex sections to maintain electrical trace isolation during the assembly. The second-generation ML arrays fit well within a 9F distal tip construction. Thus far, 5 second-generation ML array assemblies have been fabricated and tested and are currently being integrated with 9F catheter shafts (Figure 2).

### Simulation and Bench Testing of the ML Array Designs

The first-generation ML catheter arrays showed only modest fractional bandwidth (FBW) performance at 25%, which was due to both poor mechanical bond lines in the array stack and an unoptimized parylene thickness. Use of the Krimholtz-Leedom-Matthaei<sup>35</sup> acoustic transducer model revealed that the parylene layer, although needed for electrical isolation with biological tissue, is undesirable in this design for thicknesses beyond a few micrometers. An optimized parylene thickness of 10  $\mu\text{m}$  was elected to achieve complete coverage without pinhole problems and with only a 0.6-dB loss in signal sensitivity and a 7% loss in maximum design bandwidth. With improved assembly techniques and optimization of the rudimentary matching layer, the second-generation devices have shown FBW performance in the 50% range. Array per-

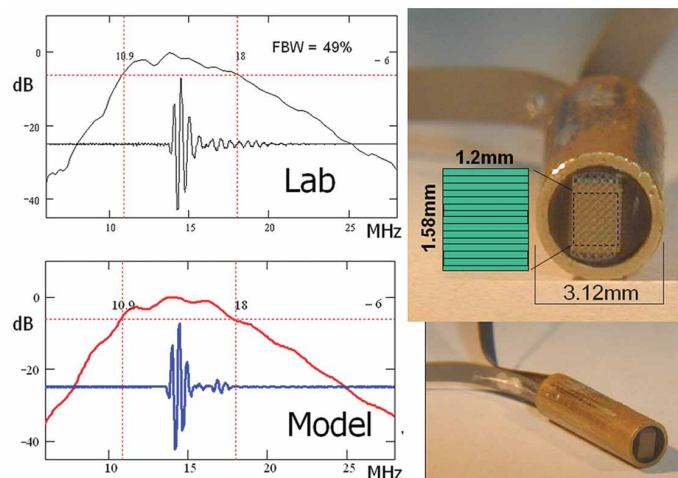


**Figure 2.** The second-generation 14.4-MHz ML piezoceramic 9F subassembly is shown (right) with measured (top left) and estimated (bottom left) pulse echo performance. Fifty percent FBW was achieved. The array aperture of only 1.2  $\times$  1.58 mm is shown (top right) with the element layout as indicated.

formance simulations agreed well with these new devices, as shown in Figure 2. Two-way pulse echo data from a flat X-cut quartz reflector at 3.75 mm from the array in water were collected with a standard pulse generator (5900PR; GE Panametrics, Waltham, MA; 2  $\mu\text{J}$  of energy) and a fast sampling oscilloscope (LC534; LeCroy, Chestnut Ridge, NY; 500 megasamples per second). A direct image comparison with a commercial 10-MHz phased array sector probe with elevation focusing was made to confirm that imaging parameters were working well on the Vivid 7 Dimension commercial imaging system (Figure 3).

### Pig Experiments

The prototype ML array was used in studies of 4 adult (34- to 55-kg) pigs, in 3 of which imaging was performed from the right atrium and right ventricle to study ablation procedures performed in right-sided locations. In the fourth animal, the catheter was inserted into the right ventricle only, close to the septum, for visualizing ablation on the left septal surface.

Closed-chest pigs were studied under general anesthesia with 2% isoflurane and mechanical ventilation. Electrocardiography, body temperature, and oxygen saturation were monitored; femoral arteries and veins as well as jugular veins were exposed by surgical incision in preparation for

catheter insertion. The Animal Care Committees of Oregon Health & Science University and the University of California, Los Angeles, approved the scientific methods and the animal treatment procedures.

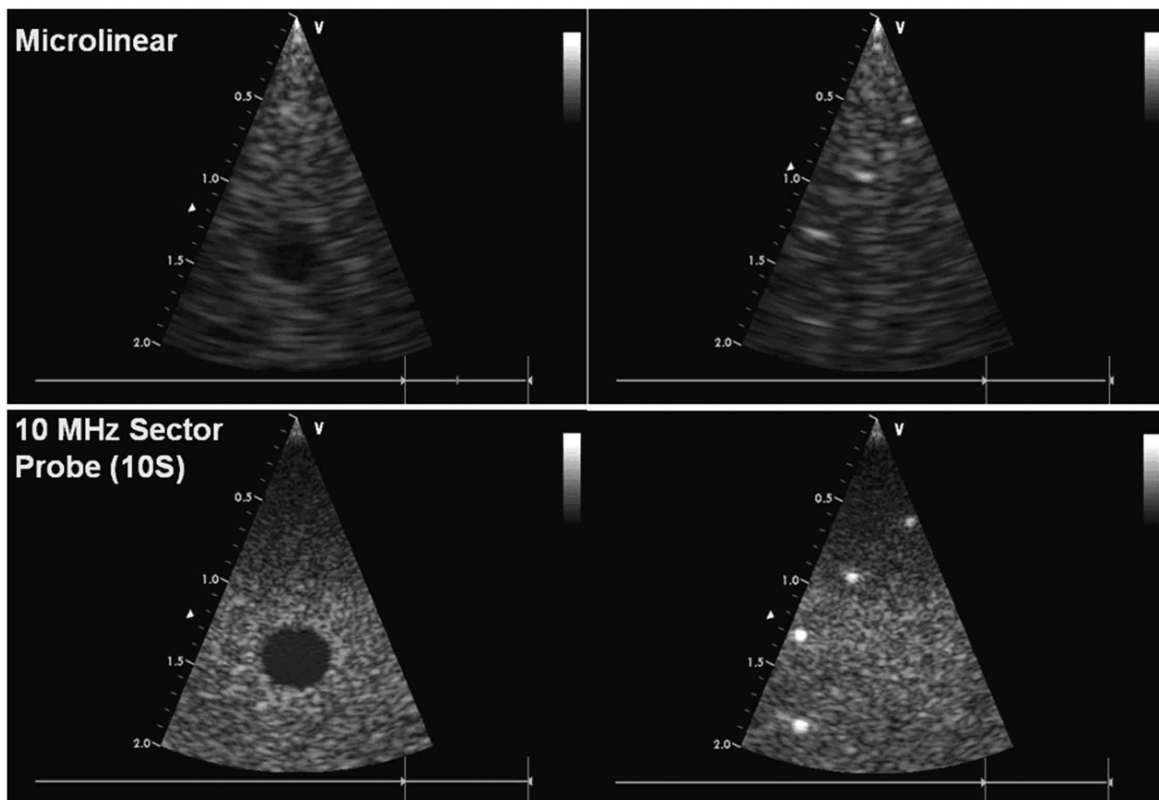
In vivo placements of an RFA device were guided by visualization from the ML probe; in 1 particular case, a small integrated ablation wire deployed directly from the tip of an experimental combination ML catheter was tracked by the ML catheter (Figure 4B) during attempts at tissue ablation. Catheter ablations were otherwise performed with a Livewire catheter with a 4-mm tip (St Jude Medical) at 4 locations in the isthmus area or the right ventricle in 3 of the pigs and in 3 locations in the left ventricle in the fourth pig. Ablation was accomplished with a Stockert RF generator (Biosense Webster, Inc). The target temperature was 55° to 70°C, and the duration of delivery was 60 seconds, with power of 50 W.

Imaging characteristics as well as changes in strain mechanics were obtained in the Doppler strain imaging mode with the ML catheter operated through the Vivid 7 Dimension system at a transducer frequency of 12 MHz. High-frame rate gray scale images (120 frames per second) were also obtained and processed offline with a 2D strain program for detecting alterations of cardiac mechanics associated with ablation in EchoPac software (GE Vingmed Ultrasound AS).

**Results**

Along with a total imaging depth of field of at least 2.5 cm, the steerability and forward-looking nature of this catheter made it easy to bring it into proximity with the ablation catheter and set up for imaging ablation within 1 minute of attempted manipulation and only 2 or 3 short fluoroscopic bursts. There was little difference in

**Figure 3.** Phantom image test comparison with a commercial probe. The 14-MHz, 24 element ML catheter array (top) with its limited aperture compares reasonably well with the much larger-aperture neonatal probe, the Vingmed 10S (GE Vingmed Ultrasound SA; bottom), which is a 10-MHz high-frequency phased array equipped with 64 elements. Both arrays were tested here on the Vivid 7 Dimension imaging system.



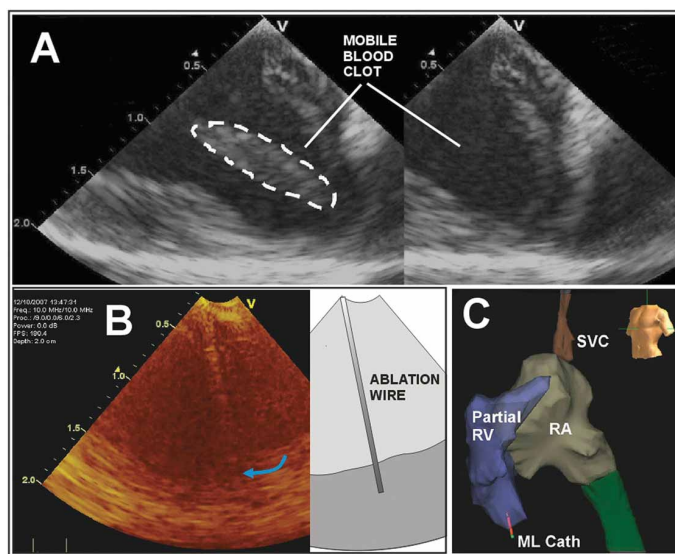
the ability to visualize ablation from the right ventricle and within the right ventricle compared with visualization from the right ventricle of septal ablation on the left ventricular side. Figure 4A shows the general near-field image quality of a mobile blood clot, the imaging of a special ablation wire that had been specially integrated in a side channel of one of the ML designs, and as well a NavX electroanatomic mapping result of the right heart with the ML clearly delineated near the apex of the right ventricle.

Ablation could be localized by tissue brightening along with the expected bubble formation from gas evolution<sup>36</sup> during tissue heating, as illustrated in Figure 5, and by the substantial diminution of regional strain for both 2D strain computation and the strain rate determined online by tissue Doppler imaging, as shown in Figure 6. The RF shielding of the ML imaging catheter was adequate in the sense that any minor RF noise interferences observed in the ultrasound images were localized to brightening and reverberation in the far field, which were generally away from near-field views of ablation sites. In addition, imaging noise from ablation activity was minimal in the ML forward-looking catheter compared with our side-looking (unshielded) hockey stick design.

Ablation sites in 3 of the 4 pigs were verified by pathologic examination after the animals were terminated (Figure 7).

## Discussion

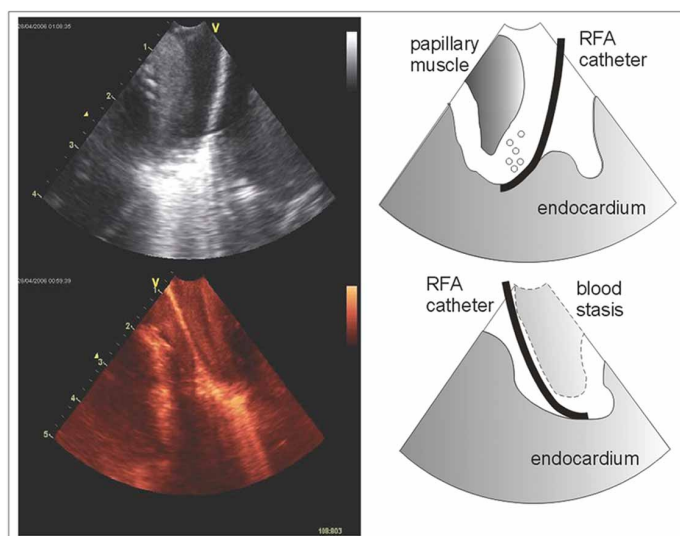
We previously reported on the first of 3 devices built in this program, a piezoelectric ceramic side-looking 9F catheter called the hockey stick. In concept, its design as a side-looking imaging device was not unlike the AcuNav catheter, although efforts to produce it preceded the introduction of that product. Both our side-looking phased array intracardiac imaging catheter and the forward-looking ML catheter have satisfactorily agile handling, built with the inherent directional steerability of EP catheters. The EP-enabled capability has permitted recording of intracardiac electrical potentials, although not under visualization of the array, because the EP electrodes were mounted at the tip and behind the array. These enabling electrodes, however,



**Figure 4.** The ML in vivo imaging image quality is shown in **A** with a display depth of 2 cm. A special ablation wire is tracked in **B**, and the ML catheter tip 3D spatial position in the apical region of the right ventricle (RV) is tracked dynamically in **C** with a partially completed volumetric map of the right side of the pig heart from the NavX electroanatomic mapping system. Note the ML catheter tip shown near the RV apex at the bottom left in **C**. RA indicates right atrium.

used in both the hockey stick and the ML catheters, have allowed very straightforward integration with the NavX mapping system for 3D electroanatomic spatial localization.

**Figure 5.** Ablation visualized in the right ventricular apex. From the onset of the activation of the RFA energy, the tip of the ablation catheter generates a brightened tissue signal created by tissue gas bubble evolution.



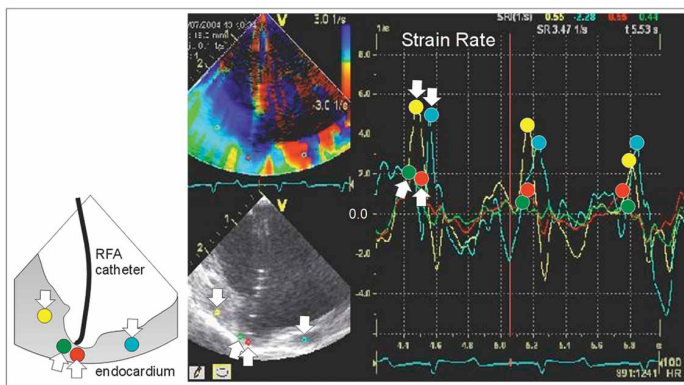
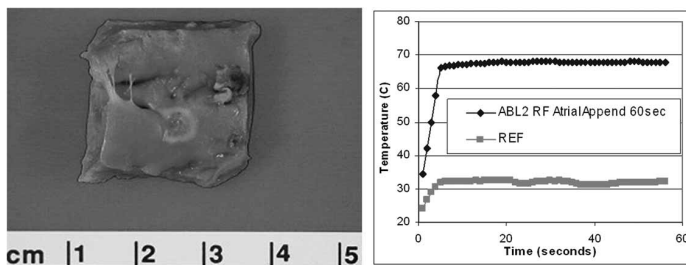


**Figure 6.** Strain rate imaging after ablation. The cup-shaped tissue depression beneath the flexible ablation tip has decreased strain, as shown by the time course of the red and green traces. The yellow and turquoise traces (with downward arrows) show a noticeably greater peak strain rate than the red and green traces (with peaks at the upward arrows). The diminution in the strain rate of this region was still present after the ablation catheter had been moved away.

A key limitation in the optimal integration of the NavX system and the side-looking device has been the necessity of preparing a specially segmented electrode on the catheter shaft to permit a continuous electroanatomic computation of the shaft’s angular position, which would produce the 3D geometric position of the array’s image plane. Plans are under way for this extended NavX integration in both the ML and the hockey stick catheter designs, which will be particularly valuable for localization of the ML image plane as a small field-of-view device.

The ML catheter represents a very high-frequency, near-field-optimized, forward-looking intracardiac device that operates without special software on a standard commercial imaging sys-

**Figure 7.** An ablation lesion created on the endocardial surface of the right atrial appendage is shown (left) with the ablation site temperature plot (right). To confirm tissue temperatures during ablation, a pair of 0.5-mm fluoroptic temperature probes (Luxtron Corp, Santa Clara, CA) were placed within the myocardium.



tem. It incorporates the same dynamic steerability that was designed into the side-viewing hockey stick, which aids navigation. Additional planned steps in the evolution of this technology will include completion of a thermally efficient cMUT array capable of delivering high-intensity focused ultrasound for ablation, integrating imaging with therapy in the same device.

### References

- Lloyd-Jones DM, Wang TJ, Leip EP, et al. Lifetime risk for development of atrial fibrillation: the Framingham Heart Study. *Circulation* 2004; 110:1042–1046.
- Cappato R, Calkins H, Chen SA, et al. Worldwide survey on the methods, efficacy, and safety of catheter ablation for human atrial fibrillation. *Circulation* 2005; 111:1100–1105.
- Drant SE, Klitzner TS, Shannon KM, Wetzel GT, Williams RG. Guidance of radiofrequency catheter ablation by transesophageal echocardiography in children with palliated single ventricle. *Am J Cardiol* 1995; 76:1311–1312.
- Görge G, Ge J, Baumgart D, von Birgelen C, Erbel R. In vivo tomographic assessment of the heart and blood vessels with intravascular ultrasound. *Basic Res Cardiol* 1998; 93: 219–240.
- Lai WW, Al-Khatib Y, Klitzner TS, et al. Biplanar transesophageal echocardiographic direction of radiofrequency catheter ablation in children and adolescents with the Wolff-Parkinson-White syndrome. *Am J Cardiol* 1993; 71:872–874.
- Lesh MD, Kalman JM, Karch MR. Use of intracardiac echocardiography during electrophysiologic evaluation and therapy of atrial arrhythmias. *J Cardiovasc Electrophysiol* 1998; 9(suppl):S40–S47.
- Chu E, Fitzpatrick AP, Chin MC, Sudhir K, Yock PG, Lesh MD. Radiofrequency catheter ablation guided by intracardiac echocardiography. *Circulation* 1994; 89:1301–1305.
- Shpun S, Gepstein L, Hayam G, Ben-Haim SA. Guidance of radiofrequency endocardial ablation with real-time three-dimensional magnetic navigation system. *Circulation* 1997; 96:2016–2021.
- Kadish A, Hauck J, Pederson B, Beatty G, Gornick C. Mapping of atrial activation with a noncontact, multielectrode catheter in dogs. *Circulation* 1999; 99:1906–1913.
- Gornick CC, Adler SW, Pederson B, Hauck J, Budd J, Schweitzer J. Validation of a new noncontact catheter system for electroanatomic mapping of left ventricular endocardium. *Circulation* 1999; 99:829–835.
- Schwartz SL, Pandian NG, Kusay BS, et al. Real-time intracardiac two-dimensional echocardiography: An experimental study of in vivo feasibility, imaging planes, and echocardiographic anatomy. *Echocardiography* 1990; 7:443–455.

12. Olgin JE, Kalman JM, Chin M, et al. Electrophysiological effects of long, linear atrial lesions placed under intracardiac ultrasound guidance. *Circulation* 1997; 96:2715–2721.
13. Hirshfeld JW Jr, Balter S, Brinker JA, et al. ACCF/AHA/HRS/SCAI clinical competence statement on physician knowledge to optimize patient safety and image quality in fluoroscopically guided invasive cardiovascular procedures: a report of the American College of Cardiology Foundation/American Heart Association/ American College of Physicians Task Force on Clinical Competence and Training. *J Am Coll Cardiol* 2004; 44:2259–2282.
14. Dairywala IT, Li P, Liu Z, et al. Catheter-based interventions guided solely by a new phased-array intracardiac imaging catheter: In vivo experimental studies. *J Am Soc Echocardiogr* 2002; 15:150–158.
15. Packer DL, Stevens CL, Curley MG, et al. Intracardiac phased-array imaging: Methods and initial clinical experience with high resolution, under blood visualization, initial experience with intracardiac phased-array ultrasound. *J Am Coll Cardiol* 2002; 39:509–516.
16. Ren JF, Marchlinski FE, Callans DJ, Herrmann HC. Clinical use of AcuNav diagnostic ultrasound catheter imaging during left heart radiofrequency ablation and transcatheter closure procedures. *J Am Soc Echocardiogr* 2002; 15: 1301–1308.
17. Zong H, Lacomis JM, Schwartzman D. On the accuracy of CartoMerge for guiding posterior left atrial ablation in man. *Heart Rhythm* 2007; 4:595–602.
18. Daccarett M, Segerson NM, Günther J, et al. Blinded correlation study of three-dimensional electro-anatomical image integration and phased array intra-cardiac echocardiography for left atrial mapping. *Europace* 2007; 9: 923–926.
19. Fahmy TS, Mlcochova H, Wazni OM, et al. Intracardiac echo-guided image integration: Optimizing strategies for registration. *J Cardiovasc Electrophysiol* 2007; 18:276–282.
20. Martinek M, Nesser HJ, Aichinger J, Boehm G, Purerfellner H. Impact of integration of multislice computed tomography imaging into three-dimensional electroanatomic mapping in clinical outcomes, safety, and efficacy using radiofrequency ablation for atrial fibrillation. *Pacing Clin Electrophysiol* 2007; 30:1215–1223.
21. Gepstein L, Hayam G, Ben-Haim SA. A novel method for nonfluoroscopic catheter-based electroanatomical mapping of the heart, in vitro and in vivo accuracy results. *Circulation*, 1997; 95:1611–1622.
22. Wittkamp FH, Wever EF, Derksen R, et al. Localisa: New technique for real-time 3-dimensional localization of regular intracardiac electrodes. *Circulation* 1999; 99:1312–1317.
23. Earley MJ, Showkathali R, Alzetani M, et al. Radiofrequency ablation of arrhythmias guided by non-fluoroscopic catheter location: a prospective randomized trial. *Eur Heart J* 2006; 27:1223–1229.
24. Kennedy JE, ter Haar GR, Cranston D. High intensity focused ultrasound: surgery of the future? *Br J Radiol* 2003; 76:590–599.
25. Lubbers J, Hekkenberg RT, Bezemer RA. Time to threshold (TT): a safety parameter for heating by diagnostic ultrasound. *Ultrasound Med Biol* 2003; 29:755–764.
26. Pham PP, Balaji S, Shen I, Ungerleider R, Li X, Sahn DJ. Impact of conventional versus biventricular pacing on hemodynamics and tissue Doppler imaging indexes of resynchronization postoperatively in children with congenital heart disease. *J Am Coll Cardiol* 2005; 46:2284–2289.
27. Li XK, Pemberton J, Thomenius K, et al. Development of an electrophysiology (EP)-enabled intracardiac ultrasound catheter integrated with NavX 3-dimensional electrofield mapping for guiding cardiac EP interventions: experimental studies. *J Ultrasound Med* 2007; 26:1565–1574.
28. Stephens DN, Cannata J, Liu R, et al. The acoustic lens design and in vivo use of a multifunctional catheter combining intracardiac ultrasound imaging and electrophysiology sensing. *IEEE Trans Ultrason Ferroelectr Freq Control* 2008; 55:602–618.
29. Smith SW, Light ED, Wolf PD. Feasibility study of in vivo real-time 3D intracardiac ultrasound [abstract]. *J Am Coll Cardiol* 1999; 33(suppl):405A.
30. Back MR, Kopchok GE, White RA, et al. Forward-looking intravascular ultrasonography: In vitro imaging of normal and atherosclerotic human arteries. *Am Surg* 1994; 60:738–743.
31. Gatzoulis L, Watson RJ, Jordon LB, et al. Three-dimensional forward-viewing intravascular ultrasound imaging of human arteries in vitro. *Ultrasound Med Biol* 2001; 27:969–982.
32. Light ED, Idriss SF, Wolf PD, Smith SW. Real-time three-dimensional intracardiac echocardiography. *Ultrasound Med Biol* 2001; 27:1177–1183.
33. Lee W, Idriss SF, Wolf PD, Smith SW. A miniaturized catheter 2-D array for real-time, 3-D intracardiac echocardiography. *IEEE Trans Ultrason Ferroelectr Freq Control* 2004; 51:1334–1346.
34. Nikoozadeh A, Wygant I, Lin D, et al. Fully integrated cMUT-based forward-looking intracardiac imaging probe for electrophysiology. In: *Proceedings of the IEEE International Ultrasonics Symposium*. Piscataway, NJ: Institute of Electrical and Electronics Engineers; 2007: 900–903.
35. Krimholtz R, Leedom D, Matthaei G. New equivalent circuit for elementary piezoelectric transducers. *Electron Lett* 1970; 6:398–399.
36. Marrouche NF, Natale A. Monitoring pulmonary vein isolation using phased array intracardiac echocardiography in a patient with atrial fibrillation. *Electromedica* 2002; 70:77–80.